Thermal radiation from C_N^+ and La@C_N^+

M. Hedén, K. Hansen,[a] F. Jonsson, E. Rönnow, A. Gromov, and E. E. B. Campbell
Department of Physics, Göteborg University, SE-41296 Göteborg, Sweden

A. Taninaka and H. Shinohara
Department of Chemistry, Nagoya University, Nagoya 464-8602, Japan

(Received 28 February 2005; accepted 11 April 2005; published online 3 August 2005)

The radiative cooling of positively charged fullerene and endohedral fullerene fragments of C_{60}, C_{70}, C_{84}, and La@C_{82} has been measured in a time-of-flight mass spectrometer. The radiative cooling is measured via its influence on the metastable decay. The emissivity extracted from the data is between 4×10^{-4} and 13×10^{-4}. These values agree fairly well with the emissivity calculated from considering the low-energy tail of the surface plasmon. No major difference is found in the emission behavior of empty and endohedral fullerenes. © *2005 American Institute of Physics*.
[DOI: 10.1063/1.1925277]

I. INTRODUCTION

Fullerenes belong to a small class of clusters which, when thermally excited, exhibit three competing cooling mechanisms, viz., neutral fragmentation, electron emission, and emission of photons. Experimentally, these three decay channels are observed at time scales characteristic for time-of-flight mass spectrometers, i.e., on the order of microseconds. The reason for the simultaneous emission of thermal electrons and neutral fragments (C_2) on these time scales is well understood by now as a relatively mild condition on the values of the parameters characterizing the two thermal processes, i.e., the frequency factors and the activation energies. The branching ratio between these two processes changes only slowly with the time scale of the measurement, essentially as a power law in time, with a small power. This is a consequence of the similar nature of the two channels, which proceed via activated processes.

Fullerenes have become something of a model system for the dynamics of highly excited molecules with a large number of degrees of freedom. However, if detailed studies of fragmentation and electron emission are to be performed accurate modeling of the third decay channel, photon emission, is essential. Photon emission is in general not an activated process and has a much weaker dependence on the excitation energy. In the simplest situation, where the photon absorption cross section is temperature independent and nonvanishing at low energies, the emission rate constant mainly depends on the factors associated with the phase space of the emitted photon. Consequently radiative cooling dominates at low excitation energies, and there is a transition from particle emission to radiative cooling on some time scale. With a reasonably accurate parametrization of the activated processes, it is possible to use experimental measurements of this crossover as a probe of the radiative cooling, which otherwise poses a difficult experimental problem. Essentially the activated process, which in the experiments described below is C_2 emission, acts as a calorimeter which samples the energy content of the cluster.[1] One may alternatively consider the photon emission to be the best-known process, and use this to gain information on the activated process. This is the approach used in Ref. 2. These results are complementary to those obtained in Ref. 1 and those reported here, and will be discussed in order to assess the consistency of the extracted parameters.

The influence of an atom inside the fullerene cage will also be investigated. There is a large family of endohedral fullerenes with properties, such as stability and electronic structure, different from the empty fullerenes. Whether the extent of thermal radiation differs in such molecules is not a trivial question. The main aim of the work presented here was to investigate this.

The paper starts with a presentation of the experimental procedure, followed by the initial data analysis and results. The parameters of the radiative cooling are extracted from the data and the results compared with literature values of both experimental and theoretical nature.

II. EXPERIMENTAL PROCEDURE

The equipment has been described previously.[1] Briefly, fullerenes are vaporized from a resistively heated oven and ionized with an UV laser in the acceleration region of a reflectron-time-of-flight (RETOF) mass spectrometer. The ions are extracted with an acceleration field which is switched on at a variable delay (0–7 μs) after the laser pulse. The variable delay changes the cooling time of the excited fullerenes before extraction. The amount of metastable fragmentation after the initial acceleration and before the entry into the reflectron is measured by the standard method of detuning the reflectron fields so that the ions that fragment in the first field-free region end up in a peak between the prompt peaks. The only major difference from Ref. 1 is the laser, which was a XeCl laser ($\lambda=308$ nm), whereas a N_2 laser ($\lambda=337$ nm) was used here. The former had sufficient pulse energy to cause a large degree of fragmentation of the fullerenes. The N_2 laser has a typical fluence of

[a]Electronic mail: klavs@fy.chalmers.se

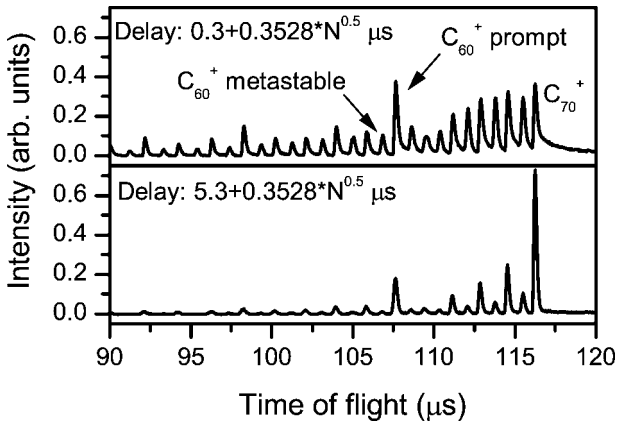

FIG. 1. Time-of-flight mass spectra of C_{70} for delays of the pulsed extraction fields of 0.3 and 5.3 μs.

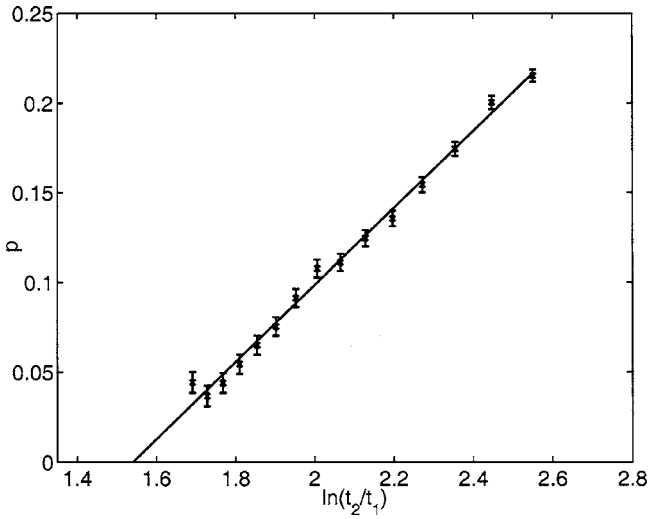

FIG. 2. Measured metastable fractions for C_{60}^{+} originating from C_{70} as a function $\ln(t_2/t_1)$ and a linear fit of the experimental data weighted with the error.

200 mJ/cm^2 in the center of the extraction region which limits the amount of absorbed energy. This has consequences for the data analysis, and will be discussed below.

The molecules investigated here are the fragment ions of the source materials C_{60}, C_{70}, C_{84}, and La@C_{82}. The C_{60} and C_{70} was commercial (purity of 99.8% and 98%+, respectively) and the C_{84} was purified from extract of fullerene soot with high-pressure liquid chromatography. The contamination of the signal from C_{60} present in the source material is small. This conclusion is based both on the observation that high-purity C_{60} and C_{70} source materials give comparable signals at the temperatures and photon energies used, and on the fact that the delayed ionization tail on the C_{60} is strongly suppressed compared with the spectra from high-purity C_{60} source material. The La@C_{82} was produced and purified as described in Ref. 3 and 4. For each source material the experiments were repeated in a number of different experimental runs each included several measurements of the spectra at about ten different delays. The (1σ) error bars in the data all refer to the measured statistical errors in these runs.

III. RESULTS AND FIRST ANALYSIS

An example of the TOF spectra for C_{60} as a source material is shown in Fig. 1 for two different delay times. For intensity reasons, the delays were restricted to values up to 7 μs for all fullerenes. As expected, the metastable fragmentation ratio decreases with increasing delay time. The metastable fragmentation ratio was extracted from the time-of-flight spectra as the area of the metastable peak divided by the sum of the area of the parent peak and the metastable peak, similar to the procedure used in Ref. 1. The definition of the area over which the peaks should be integrated involves a determination of the base line and of the separating point between the prompt fragment and the metastable fragment on one hand, and between the parent peak and the metastable peak on the other. The spectra were not background-free and the peaks were integrated after background subtraction. The background is due to delayed ionization for certain sizes, and to the effects of metastable fragmentation during the initial acceleration. Both of these phenomena give a tail to longer times. The background was determined by locating the lowest point between two neighboring peaks and connecting these. For consistency, these points were also used to define the peak integration limits. The definition of a separation time between prompt and metastable peaks in the analysis of the TOF spectrum implicitly defines the acceleration time. Molecules fragmenting before a certain time end up in the prompt peak, whereas those that fragment later end up in the metastable peak. This means that some fraction of the acceleration time is effectively delay time, which must be added to the nominal delay set by the switching time of the acceleration fields. This contribution can be calculated with the known dimensions and fields and is always included into the delay, which is denoted t_1. The total flight time for a certain parent size from the laser pulse to the entry of the reflecting fields is denoted by t_2.

An example of the measured metastable fractions as a function of delay time is shown in Fig. 2. The choice of abscissa will be justified shortly.

IV. RADIATIVE COOLING AND ENSEMBLES

The molecules that have undergone at least one evaporation in the acceleration region before extraction have a broad but still fairly well-defined energy distribution. The broad energy distribution implies an even broader distribution of thermal decay constants. A consequence of this is that the ensemble decays nonexponentially, with a decay rate which in the absence of radiative cooling is very close to $1/t$.[5] This will give rise to a metastable fraction (the fraction which decays between times t_1 and t_2) which is the integrated decay constant;

$$p \propto \int_{t_1}^{t_2} \frac{dt}{t} = \ln(t_2/t_1) \quad \text{(no radiative cooling)}, \tag{1}$$

which explains the choice of axis in Fig. 2. Several physical effects may modify Eq. (1). One is that the decay is saturated, i.e., all, or an appreciable amount, of molecules in the ensemble decay between t_1 and t_2. This causes the curve in Fig. 2 to flatten with increasing t_2/t_1 and thereby deviate from a straight line. The magnitude of t_2/t_1 for which this

happens depends on the heat capacity, and on the relative change in the dissociation energies from N to $N-2$.[6] The deviations are minor if the amount of fragmentation is well below unity. This will be the situation here, except for a few cases (C_{62} and C_{72}).

The $1/t$ decay will also be modified by radiative cooling. In Ref. 1 the effect was calculated to give a downward shift in the curve which can be related directly to the radiative cooling. We will present a comprehensive derivation of the equation here.

We parametrize the radiative cooling with the simple ansatz $k(t)=k(0)\exp(-\varphi t)$, which corresponds to an expansion of the logarithm of the rate constant in time and retaining only the linear term. The parameter φ is determined as

$$-\varphi \equiv \left.\frac{d\ln(k)}{dt}\right|_{t=0} = \frac{d\ln(k)}{dE}\frac{dE}{dt}, \tag{2}$$

where E is the excitation energy of the molecule. The comparison with macroscopic blackbody radiation is simplified if we introduce the microcanonical temperature instead of the energy.[7] The microcanonical temperature has to be modified with the finite heat bath (FHB) correction which means subtracting $D/2C_v$ from the microcanonical temperature corresponding to the parent energy (T_{MC}) so that $T=T_{\mathrm{MC}}-D/2C_v$. Then

$$\begin{aligned} -\varphi &= \frac{d\ln(k)}{dT}\frac{dT}{dt} \\ &= \frac{d\ln(k)}{dT}\frac{[-P(T_{\mathrm{Rad}})]}{C_v} \\ &= -\frac{D}{k_B T^2}\frac{P(T+D/2C_v)}{C_v}, \end{aligned} \tag{3}$$

where P is the radiatively emitted power, k_B Boltzmann's constant, C_v the heat capacity of the (parent) molecule, and D is the dissociation energy of the molecule. We have used an Arrhenius expression for the rate constant k. The temperature relevant for the emitted power P has a different finite heat bath correction ($T_{\mathrm{Rad}}=T_{\mathrm{MC}}-h\nu/2C_v$) since it concerns photon emission rather than fragment evaporation. We choose to ignore the FHB correction for T_{Rad} since the average photon energy is expected to be about 2 eV compared to the dissociation energy which is about 10 eV. Thus we write $T_{\mathrm{Rad}}=T_{\mathrm{MC}}=T+D/2C_v$. The emitted power can be expressed in terms of the emissivity, ε, as $P=\varepsilon S\sigma_{\mathrm{SB}}(T+D/2C_v)^4$, where S is the surface area of the molecule and σ_{SB} is the Stefan–Boltzmann constant. Then φ becomes

$$\varphi = \frac{D\varepsilon S\sigma_{\mathrm{SB}}(T+D/2C_v)^4}{C_v k_B T^2}. \tag{4}$$

This value will be taken constant for each molecule, i.e., independent of temperature. We can estimate the validity of this approximation by calculating the higher-order terms in Eq. (2). With an emitted power of αT^6, the next-to-leading order term is (ignoring finite-heat-bath corrections)

$$\frac{d^2\ln(k)}{dt^2} = -\frac{d\varphi}{dt} = -\varphi^2\frac{4k_B T}{D}. \tag{5}$$

The ratio $4k_B T/D$ is on the order of $1/8$ (see below). Hence, to second order

$$k \approx k(t=0)\exp\left[-\varphi t - \tfrac{1}{16}(\varphi t)^2\right]. \tag{6}$$

When $t=2/\varphi$, say, the decay constant is hence reduced to 10% of the initial value, and the decay is virtually quenched. The second-order term at this time is still only $1/4$ in absolute terms and $1/8$ relatively. We can therefore to a good approximation ignore this contribution and use the leading order term alone.

Both D and ε will in general depend on the molecule. The surface area S is calculated using the molecular radius of C_{60} and scaled to be proportional to the number of atoms in the molecule. The heat capacity is assumed to be equal to $C_v=(3N-6)k_B$.[8] Equation (3) allows us to calculate the survival probability, $\rho(E,t)$, for a molecule which starts with a specific energy and hence rate constant at time zero, $k(t=0)$, as

$$\begin{aligned} \frac{d\rho(E,t)}{dt} &= -k(E,t)\rho(E,t) \\ &= -k(E,0)e^{-\varphi t}\rho(E,t) \Rightarrow \rho(E,t) \\ &= \rho(E,0)e^{-[k(E,0)](1-e^{-\varphi t})/\varphi}. \end{aligned} \tag{7}$$

We can now calculate $\rho(E,t)$ for a given $\rho(E,0)$. One can use different conventions about the energy in the argument of this function. The direct approach is to use the actual energy, i.e., including the effect of radiative cooling as in Ref. 1. Alternatively one may choose to represent the function in terms of the energy the molecule would have in the absence of radiative cooling and use an external factor correcting for the radiative energy loss. We will adopt the latter convention here, which also means that we can drop the time argument in ρ.

For size N the energy distribution contains a high-energy cutoff given by the survival probability calculated in Eq. (7):

$$f_+(E,t) = e^{-[k_N(E,0)](1-e^{-\varphi_N t})/\varphi_N}. \tag{8}$$

The precursor molecule, $N+2$, has a similar cutoff. This cutoff defines the upper limit of the precursor energy and by energy conservation, also a lower-energy cutoff for N. This contributes a factor

$$f_-(E,t) = 1 - e^{-[k_{N+2}(E+D_{N+2},0)](1-e^{-\varphi_{N+2}t})/\varphi_{N+2}}. \tag{9}$$

The combined effect of f_+ and f_- is the product:

$$\begin{aligned} f(E,t) &= \rho(E,0)f_+f_- \\ &= \rho(E,0)e^{-[k_N(E,0)](1-e^{-\varphi_N t})/\varphi_N} \\ &\quad\times\left\{1 - e^{-[k_{N+2}(E+D_{N+2},0)](1-e^{-\varphi_{N+2}t})/\varphi_{N+2}}\right\}. \end{aligned} \tag{10}$$

This is the distribution for molecules which have not yet been size selected. With increasing energy it increases abruptly from zero at the lower cutoff and reaches the value $\rho(E,t)$. At the higher cutoff about D_N above the lower cutoff it decreases abruptly to zero again. Once the molecules are

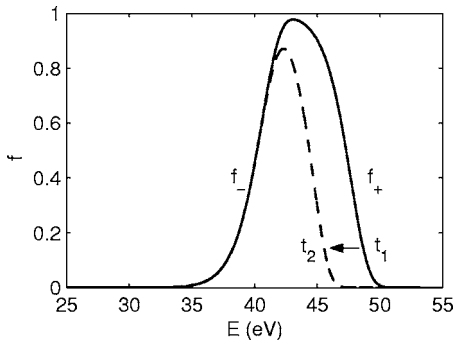

FIG. 3. Calculated internal energy distributions according to Eq. (10) for C_{50}^+ at times $t_1=3.55$ μs and $t_2=t_1+45.21$ μs. The part in between the two right flanks of the two curves is the fraction that will decay during the first field-free flight time and thus end up in a metastable peak in the mass spectrum. The dissociation energy is set to 8.8 eV, the Arrhenius preexponential factor to 2×10^{19} s^{-1} and the emissivity $\varepsilon=7\times10^{-4}$, and the value of E' from the caloric curve is set to 7.53 eV.

size selected during the latter stage of the acceleration, at $t=t_1$, the low-energy cutoff (given by f_-) freezes, whereas the high-energy cutoff (determined by f_+) keeps developing as illustrated in Fig. 3.

The general solution of Eq. (10) is not easy. We will make the assumption that the low-and the high-energy cutoffs are well separated, so that f_- is close to unity for all the energies where f_+ is less than unity. This means that we can calculate the (unnormalized) metastable fragmentation rate as the motion of the high-energy cutoff with time. At a given time t_i, the cutoff energy E_i is determined as the solution of the equation

$$\frac{k_N(E_i,0)}{\varphi_N}(1-e^{-\varphi_N t_i})=1, \tag{11}$$

which gives the point where the derivative of f_+ has its maximum. The factor $(1-e^{-\varphi_N t_i})/\varphi_N$ has the dimension of time and combined with the Arrhenius expression for the rate constant, $k_N=A\exp[-D_N/k_BT(E)]$, as well as a caloric curve for the molecule, $E=C_vT+E'$, we get the following expression for the cutoff energies:

$$E_i=\frac{C_vD_N}{k_B\ln\left[\dfrac{A}{\varphi_N}(1-e^{-\varphi_N t_i})\right]}+E'. \tag{12}$$

Hence the metastable fraction is

$$p\propto\int_{E_2}^{E_1}\rho(E)dE, \tag{13}$$

where E_1 and E_2 are given in Eq. (12) at times t_1 and t_2, respectively.

In the simplest case $\rho(E)$ is a constant and we will consider this first. Then

$$p\propto\frac{C_v}{k_B\ln\left[\dfrac{A}{\varphi_N}(1-e^{-\varphi_N t_1})\right]}-\frac{C_v}{k_B\ln\left[\dfrac{A}{\varphi_N}(1-e^{-\varphi_N t_2})\right]}, \tag{14}$$

where a division by D_N has been done to account for the width of the distribution in an average way. This expression can be simplified if we assume that the radiative cooling is small on the time scale of t_1, or more precisely that $\varphi_N t_1$ is small. A change of variables to $r\equiv t_1/t_2$ and $\Delta\equiv\varphi_N(t_2-t_1)$ [or $t_2=\Delta/[\varphi_N(1-r)]$ and $t_1=\Delta r/[\varphi_N(1-r)]$] allows an expansion in the small parameter r. Equation (14) is rewritten as

$$p\propto\frac{C_v\ln\left[\dfrac{1-e^{-\Delta/(1-r)}}{1-e^{-\Delta r/(1-r)}}\right]}{k_B\ln\left[\dfrac{A}{\varphi_N}(1-e^{-\Delta/(1-r)})\right]\ln\left\{\dfrac{A}{\varphi_N}[1-e^{-\Delta r/(1-r)}]\right\}}. \tag{15}$$

Expanding the numerator of p in the small quantity r gives

$$\ln\left[\frac{1-e^{-\Delta}}{\Delta}\frac{1-\dfrac{\Delta re^{-\Delta}}{1-e^{-\Delta}}}{r}\left(1-\frac{1}{2}r\Delta\right)\right]\approx\ln\left(\frac{1-e^{-\Delta}}{\Delta}\right)+\ln(1/r), \tag{16}$$

where the terms left out are on the order of r relative to the smallest term retained. The two factors in the denominator can be approximated as

$$\ln\left[\frac{A}{\varphi_N}(1-e^{-\Delta})\right]\equiv G', \tag{17}$$

and

$$\ln\left[\frac{A}{\varphi_N}\Delta r\right]\approx\ln(\omega t_1)\equiv G. \tag{18}$$

The first factor, involving only Δ, is a constant in these experiments. The second, $\ln(At_1)$, depends on t_1 but only very weakly because A is so much larger than $1/t_1$. Hence we have

$$p\propto\frac{C_v}{k_BG'G}\left[\ln(t_2/t_1)+\ln\left(\frac{1-e^{-\Delta}}{\Delta}\right)+O(r)\right], \tag{19}$$

where the definition of r was reintroduced. This result is similar to the one derived in Ref. 1, apart from a term Δ which was erroneously introduced there, as pointed out by J. U. Andersen. The value of the Gspann parameter G depends on the measurement time, as indicated with the primed versus nonprimed value above. The present derivation specifies the precise times which are relevant for this quantity in these experiments. The difference between G and G' is small, about 4%–5%, and we will use $G=G'=31$ for comparison with Ref. 1.

V. EFFECT OF NONCONSTANT ENERGY DISTRIBUTIONS

The above results are derived assuming that the energy distribution ρ is constant, and it must be modified when this is not the case. The mass distribution indicates that such a correction is relevant here. The envelope of the mass abundance distribution is not flat, but decreases with the number of carbon atoms lost. An abundance distribution which decreases with the number of lost atoms indicates that the distribution of the initially absorbed energy is not flat but rather decreases with increasing energy. This idea was successfully applied to describe the relation between internal energy and the fragmentation pattern of C_{60}.[9] The nonconstant energy distribution will change the result of the integration in Eq. (13) and influence the fit of Δ from the experimental data.

We express the energy dependence of ρ in exponential form:

$$\rho(E) = ce^{-\alpha E}, \tag{20}$$

where c is a constant. This is an approximation and the value of α will in general depend on the size of the molecule,[9] but we will that assume it is constant over the 8–10-eV energy interval spanned by one cluster size. The value of α was extracted from the experimental data as

$$\alpha = -\frac{1}{D_N}\frac{d\ln(I_N)}{dN}. \tag{21}$$

The derivative was averaged over several sizes to avoid variations due to size-to-size variations of the dissociation energy. For simplicity we here used 8 eV for all D_N. Values of αD_N were 0.12–0.33.

At the mass selection time t_1, the energy distribution for size N integrates to give the abundance:

$$I_N(t_1) = c\int_{E_1-\Delta E}^{E_1} e^{-\alpha E}dE = \frac{c}{\alpha}e^{-\alpha E_1}(e^{\alpha\Delta E}-1), \tag{22}$$

where ΔE is the width of the energy distribution at t_1. A variation of t_1 does not change this width, provided radiative cooling is negligible on this time scale, $\varphi_N t_1 \ll 1$, as already assumed above in Eq. (15). The amount of metastable fragmentation between t_1 and t_2 is therefore

$$p = \frac{\int_{E_2}^{E_1}\rho(E)dE}{I_N(t_1)} = \frac{e^{\alpha(E_1-E_2)}-1}{e^{\alpha\Delta E}-1}, \tag{23}$$

where Eqs. (20) and (22) were used. The denominator is a constant. Since $\alpha\Delta E$ is small compared to unity, and $E_1 - E_2 < \Delta E$, we can expand the exponential in the numerator to second order in the energy difference to get

$$p \propto E_1 - E_2 + \frac{\alpha}{2}(E_1-E_2)^2. \tag{24}$$

We now use the results from the previous section to express the energy difference as

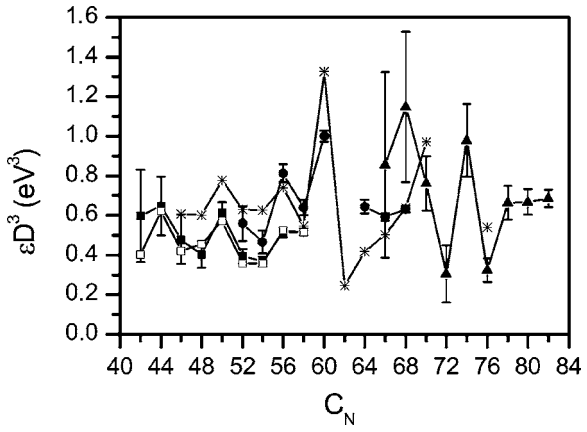

FIG. 4. Experimentally obtained values of εD^3 for ionic fullerene fragments from C_{60} (squares), C_{70} (circles), and C_{84} (triangles). The open squares are the recalculated values for C_{60} fragments from Ref. 1, as described in the text. The stars are from Ref. 18, see Eq. (29) and text for details.

$$E_1 - E_2 = \frac{C_v}{k_B G' G}\left[\ln(t_2/t_1) + \ln\left(\frac{1-e^{-\Delta}}{\Delta}\right)\right]. \tag{25}$$

For simplicity of notation we write $y \equiv \ln\{[1-\exp(-\Delta)]/\Delta\}$. Then, from Eqs. (24) and (25)

$$p \propto \ln(t_2/t_1) + y + \frac{\alpha C_v}{2k_B G' G}[\ln(t_2/t_1)+y]^2. \tag{26}$$

The correction to Eq. (19) is, to leading order in α, estimated by expanding the curve around a typical value of $\ln(t_2/t_1)$. To be specific we will use the average of the measured data for each curve, $\overline{\ln(t_2/t_1)}$, as the expansion point. This gives

$$p \propto \ln(t_2/t_1)\left\{1 + \frac{\alpha C_v}{k_B G' G}[\overline{\ln(t_2/t_1)}+y]\right\} + y + \frac{\alpha C_v}{2k_B G' G}$$
$$\times[-\overline{\ln(t_2/t_1)}^2 + y^2] \propto \ln(t_2/t_1) + y + \frac{\alpha C_v}{2k_B G' G}$$
$$\times[-\overline{\ln(t_2/t_1)}^2 + y^2 - 2\,\overline{\ln(t_2/t_1)} - 2y]. \tag{27}$$

The last term is the leading order correction to the nonconstant energy distribution. For the values relevant to our experiments, the correction has the same sign as y, i.e., the experimental intercept overestimates the value of $y = \ln\{[1-\exp(-\Delta)]/\Delta\}$. The magnitude of the correction is between 5% and 30%.

VI. DISCUSSION

From the experiments we can extract values for Δ as described above. By using the equation

$$\Delta = (t_2 - t_1)\varphi = (t_2 - t_1)\frac{D^3\varepsilon S\sigma_{SB}}{C_v k_B^3 G G'}\left(1 + \frac{G' k_B}{2C_v}\right)^4, \tag{28}$$

[where $T \approx D/(Gk_B)$ was used[10]] we get values for εD^3 as shown in Fig. 4. Measured values of φ are listed in Table I. The data on C_{60}^+ fragments from Ref. 1, displayed as open squares in Fig. 4, are reproduced very well after correcting for the nonflat internal energy distribution. The values of εD^3 for C_{56}^+–C_{58}^+ are slightly different depending on whether the source material was C_{60} or C_{70}. It most likely indicates that

TABLE I. Experimental values of the parameter φ (in 10^3 s^{-1}) for fullerene fragments starting from C_{60}, C_{70}, C_{84}, and La@C_{82}.

N	C_{60}	C_{70}	C_{84}	La@C_{82}
82			51	
80			51	42
78			51	41
76			25	37
74			76	47
72			24	35
70			60	59
68		50	91	55
66		47	69	
64		52		
62				
60		83		
58	43	54		
56	44	69		
54	32	40		
52	35	49		
50	55			
48	37			
46	45			
44	62			
42	58			

the background subtraction in the data analysis is less than perfect, due to the different contributions from the part of the signal which originates in the delayed ionization at the size considered. This contribution is different for the decay chains which originate from C_{60} and from C_{70}. The difference in the values can thus be taken as an indication of the magnitude of the systematic error committed in the data analysis.

The trend in the curve of εD^3 is that the values are, if not independent of size, then at least only oscillate around a mean value, a fact which was already obvious from the results in Ref. 1. This suggests a systematics which is reasonably independent of size. Minor fluctuations are expected due to the different temperatures of the fragments. The emissivity is temperature dependent and since we use $T \approx D/Gk_B$ the temperature of a certain fragment is proportional to its dissociation energy.

This suggests that the radiative energy loss can be described by models which do not include any detailed knowledge of absorption strengths and lines, contradicting the strongly argued conclusions in Ref. 11. We expect that part of the reason for such a simplification is that the experimental data refer to very high temperatures (above 3000 *K*), which allow a significant redistribution of oscillator strengths by a number of mechanisms, whereas data on absorption lines are measured at much lower temperatures. An example of this effect is found in the surface-plasmon resonance in sodium clusters.[12]

A model which accounts for the emissivity in terms of the surface-plasmon resonance has the potential to explain the almost constant emissivities, because this resonance usually incorporates a large part of the oscillator strength, and it is short lived, which in combination means that it has a finite and smooth absorption cross section at the relatively low energies relevant for thermal radiation. We will use the model developed by Andersen and Bonderup.[2] It is discussed in more detail below.

Measurements of metastable fragmentation and radiative cooling have been performed before. Laskin and Lifshitz did experiments very similar to the present ones but by combining a time-of-flight mass spectrometer with a quadrupole ion trap they could extend the time scale up to 100 μs.[13] They confirmed that the experiments could not be fitted by a model without radiative cooling. The fit, which included thermal radiation, used the common values for the dissociation energies and preexponential factors which at the time were on the order of 8.3 eV and 5×10^{15} Hz, respectively. A later reanalysis of the data with a more sophisticated model,[14] where consistency with previously measured breakdown curves[15] was required, gave a value for the C_{60} dissociation energy of 10.04 eV and a preexponential factor of 2.1×10^{19} Hz which is closer to the values used today. In the analysis by Lifshitz and co-workers the radiative cooling was considered to be known and dissociation energies were extracted which is complementary to our approach. The description of thermal radiation was based on the results in Ref. 11 and gives a radiative rate of $\sim6\times10^3$ Hz at an internal energy of 30 eV.

Lemaire *et al.* have investigated the effect of radiative cooling on the production of C_{58}^+ fragments from C_{60}^+ after excitation by electrons in a Fourier transform ion cyclotron resonance spectrometer.[16] They excite C_{60} with one electron to produce C_{60}^{+*} and then use one more electron to fragment the fullerene ion. With a pump-probe-type experiment, the competition between fragmentation and radiative cooling was measured. They obtain a radiative rate of 3.3×10^2 Hz after excitation by 26 eV electrons. The result is in agreement with Laskin and Lifshitz[13] (which is in the same range as our results). In the kinetic modeling of the dynamic processes they assume that it only takes emission of one photon to quench any further fragmentation, which limits the accuracy of the results.

Vostrikov *et al.* also used electrons to excite C_{60} in a crossed beam experiment and then recorded the actual emission spectrum with a monochromator.[17] In the analysis of the spectra, a modified Planck formula is used without the imaginary part of the dielectric function. The reported value for ε for C_{60} is two orders of magnitude larger than can be explained by the metastable fragmentation experiments.

Our experimental values in Fig. 4 can be compared directly to measurements of the dissociation energies of fullerenes by Tomita *et al.*[18] In that work the emissivity ε is calculated with the theoretical model described in Ref. 2, and values for the dissociation energies D_N are extracted from the quenching effect of radiation on the decay rate. The predicted radiated power from C_{60}^+ is 3.3×10^4 eV/s at 3000 K, and the radiated power is modeled to have a temperature dependence that varies with the temperature to the sixth power. Thus we can write the radiated power like βT^6 where β is a proportionality constant equal to 4.5×10^{-17} eV/K^6 s and the emissivity becomes

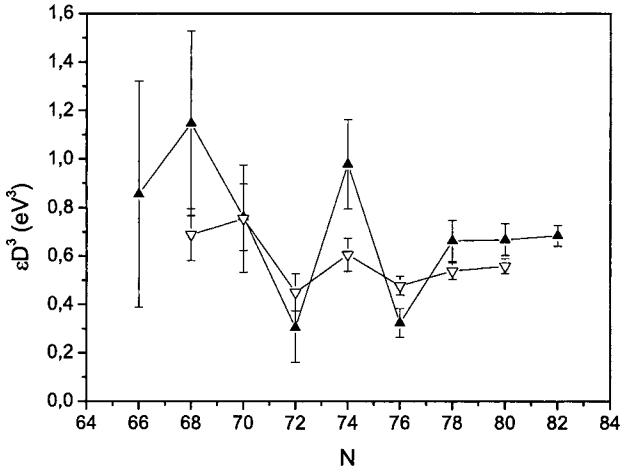

FIG. 5. Experimentally obtained values of εD^3 for ionic fullerene fragments from C_{84} (filled triangles) and La@C_{82} (open triangles). The horizontal axis gives the number of carbon atoms in the fullerene. The filled triangles are identical to those in Fig. 4 and are included for comparison.

$$\varepsilon = \frac{\beta T^6}{S\sigma_{\mathrm{SB}} T^4} \approx \frac{\beta}{S\sigma_{\mathrm{SB}}}\left(\frac{D_N}{Gk_B} + \frac{D_N}{2C_v}\right)^2. \tag{29}$$

We reconstruct the εD^3 measured in Ref. 18 with the parameters given in that paper and plot them as stars in Fig. 4. The values from Ref. 18 seem to lie a little too high for $N=46-54$, but considering the different nature of the two experiments, the agreement is fairly good.

As seen in Fig. 5 there is little difference in the εD^3 of the fullerenes, C_N^+, and the endohedrals, La@C_N^+. However, it is not possible to entirely conclude that the radiation from the two different species is the same since there could be a difference in dissociation energies. The dissociation energies for La@C_N^+ are not known exactly but measurements for La@C_{80}^+ have revealed that "the C_2 binding energies of C_{80}^+ and its endohedrals are equal within the experimental error."[19] Thus it is quite likely that there are no dramatic differences in the emissivities of the ionic fragments of C_{84} and the fragments of its endohedral relative La@C_{82}.

To extract the emissivity, the data from Fig. 4 have to be divided by their respective dissociation energies cubed. We used the relative dissociation energies from Barran *et al.*[20] normalized to 10.1 eV for C_{60}^+.[21] The emissivities are shown in Fig. 6 together with the emissivities obtained from Eq. (29). There are several other values of the dissociation energies published apart from Ref. 20. For example, Gluch *et al.* have measured the dissociation energies for fullerenes both by studying kinetic-energy release distributions[22] and metastable fractions.[23] In the analysis of both these experiments radiative cooling rates from Aarhus[2,18] have been used. Using other dissociation energies in the extraction of the emissivity above will naturally alter the values of the emissivity. From the values of φ in Table I and Eq. (28) the reader can use the desired values for the parameters S, G, D, and C_v to obtain ε.

A general expression for the emissivity can be derived with detailed balance. After a few approximations, the microcanonical expression for the photon emission rate constant can be written as

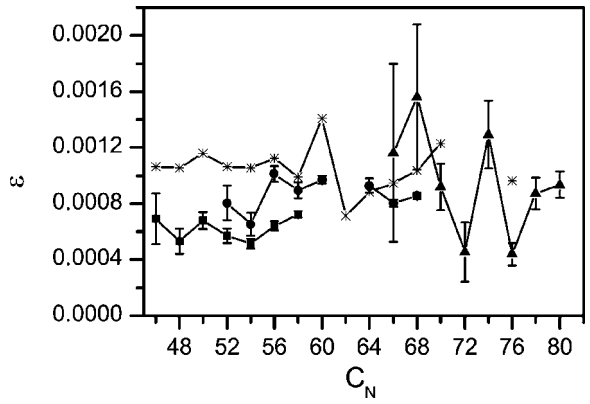

FIG. 6. Emissivities for ionic fullerene fragments estimated by dividing the experimentally determined εD^3 by their cubed dissociation energies. The squares originate from C_{60}, the circles from C_{70}, and the triangles from C_{84}. The stars are the emissivities according to Eq. (29).

$$k(E,\omega)d\omega = \frac{\omega^2}{\pi^2 c^2}\sigma(\omega)\frac{1}{e^{\hbar\omega/k_B T_{\mathrm{Rad}}} - 1}d\omega, \tag{30}$$

where ω is the angular frequency of the photon, c the speed of light, σ the photoabsorption cross section, and T_{Rad} the microcanonical temperature evaluated at the energy E.[2,18,24–26] The assumptions are that the photoabsorption cross section for a given photon energy does not change with excitation energy, and that the microcanonical temperatures of the energies E, $E-\hbar\omega/2$ and $E-3\hbar\omega/2$ can be set equal. This is equivalent to the large heat-capacity limit, and Eq. (30) therefore also resembles the Planck radiation law very closely.

The unknown quantity is the absorption cross section, σ. The model used in Ref. 2 is based on the Lorentzian shape of a two-component surface-plasmon resonance. A simplified version, which still gives correct order of magnitudes, can be calculated on the basis of a single resonance:

$$\sigma = \frac{q^2}{m_e c\epsilon_0}\gamma N_e \frac{\omega^2}{(\omega^2 - \omega_s^2)^2 + (\gamma\omega)^2}, \tag{31}$$

where q is the elementary charge, m_e is the electron mass, ϵ_0 the vacuum dielectric constant, N_e the number of valence electrons, and ω_s is the frequency of the surface-plasmon resonance.[2,24,27,28] The width of the resonance peak, γ, is set to 15 eV and the resonance frequency to $\omega_s = 20$ eV.[2,29] Using the expression for the surface plasmon in the leading order approximation gives

$$\sigma_p \propto \frac{\omega^2}{\omega_s^4}. \tag{32}$$

The emissivity is then given as

$$\varepsilon \equiv \frac{\int_0^\infty k\hbar\omega d\omega}{\int_0^\infty k(\sigma = \pi r^2)\hbar\omega d\omega}, \tag{33}$$

where r is the radius of the molecule. Performing the integrals renders a simple approximate expression for the emissivity

$$\varepsilon = \frac{40\pi q^2 \gamma N_e}{21\epsilon_0 r^2 \omega_s^4 m_e c}\left(\frac{k_B T_{\mathrm{Rad}}}{\hbar}\right)^2. \tag{34}$$

The emissivities are calculated assuming a radius of size N of 3.5 Å$N/60$, and consequently do not depend on size, apart from the very small variation due to the factor $N_e/N = (4N-1)/N$. For $T_{\mathrm{Rad}}=3500$ K, $\varepsilon=7\times10^{-4}$ is obtained for C_{60}^+.

The agreement between the data and the simplified model is generally very good when one considers the approximate nature of the model. In particular, the almost size-independent values of the emissivities are well reproduced. This holds also for the endohedral fullerene fragments. Notably, the agreement is obtained with the use of a single resonance, without using any knowledge of the detailed structures of the absorption spectra at low energies. The reason for this is twofold. The first is that the surface plasmon is expected to account for a large part of the oscillator strength in these molecules, due to the quasidelocalized nature of the valence electrons. This is analogous to the situation in metal clusters, where measurements of absolute oscillator strengths have shown that this is indeed the case.[30]

The second is the width of the resonance, which provides a strong component also close to zero energy. Note that the region below the ionization energy is inaccessible to the experiments in Ref. 29.

VII. SUMMARY

We have measured radiative cooling for ion fragments of C_{60}, C_{70}, C_{84}, and La@C_{82} by studying metastable fragmentation after laser excitation. Corrections were derived and applied for the nonconstant internal energy distribution after the laser excitation. For overlapping sizes the radiation behavior reproduces previous experiments with the same experimental equipment and in general the results compare well with other experiments on radiative cooling of fullerenes. No significant difference in the radiation behavior was found between La@C_{82}^+ fragments and the corresponding empty fullerene fragments. A simple model based on delocalized valence electrons accounts for the magnitude of the radiation and explains the absence of molecule specific radiative features.

ACKNOWLEDGMENTS

This work has been supported by the Swedish National Research Council (VR). Conversations with O. Echt are gratefully acknowledged.

[1] K. Hansen and E. E. B. Campbell, J. Chem. Phys. **104**, 5012 (1996).
[2] J. U. Andersen and E. Bonderup, Eur. Phys. J. D **11**, 413 (2000).
[3] W. Krätschmer, L. D. Lamb, K. Fostiropoulos, and D. R. Huffmann, Nature (London) **347**, 354 (1990).
[4] H. Shinohara, Rep. Prog. Phys. **63**, 843 (2000).
[5] K. Hansen, J. U. Andersen, P. Hvelplund, S. P. Møller, U. V. Pedersen, and V. V. Petrunin, Phys. Rev. Lett. **87**, 123401 (2001).
[6] K. Hansen and U. Näher, Phys. Rev. A **60**, 1240 (1999).
[7] J. U. Andersen, E. Bonderup, and K. Hansen, J. Chem. Phys. **114**, 6518 (2001).
[8] The error caused by the replacement of $3N-7$ (Ref. 7) by $3N-6$ is minor and will be ignored to be able to compare with the results in Ref. 1.
[9] K. Mehlig, K. Hansen, M. Hedén, A. Lassesson, A. V. Bulgakov, and E. E. B. Campbell, J. Chem. Phys. **120**, 4281 (2004).
[10] The Arrhenius expression for a decay is $k=Ae^{-D/k_BT} \Leftrightarrow T=D/\ln(A/k)k_B$. Assuming $k=1/t$ gives $T\approx D/\ln(At)k_B=D/(Gk_B)$.
[11] W. A. Chupka and C. E. Klots, Int. J. Mass Spectrom. Ion Processes **167/168**, 595 (1997).
[12] C. Ellert, M. Schmidt, C. Schmitt, T. Reiners, and H. Haberland, Phys. Rev. Lett. **75**, 1731 (1995).
[13] J. Laskin and C. Lifshitz, Chem. Phys. Lett. **277**, 564 (1997).
[14] J. Laskin, B. Hadas, T. D. Märk, and C. Lifshitz, Int. J. Mass. Spectrom. **177**, L9 (1998).
[15] R. Wörgötter, B. Dünser, T. D. Märk, M. Foltin, C. E. Klots, J. Laskin, and C. Lifshitz, J. Chem. Phys. **104**, 1225 (1996).
[16] J. Lemaire, M. Heninger, R. Marx, and G. Mauclaire, Int. J. Mass. Spectrom. **189**, 93 (1999).
[17] A. A. Vostrikov, A. A. Agarkov, and D. Y. Dubov, Tech. Phys. **45**, 915 (2000).
[18] S. Tomita, J. U. Andersen, C. Gottrup, P. Hvelplund, and U. V. Pedersen, Phys. Rev. Lett. **87**, 073401 (2001).
[19] T. Peres, B. Cao, H. Shinohara, and C. Lifshitz, Int. J. Mass. Spectrom. **228**, 181 (2003).
[20] P. E. Barran, S. Firth, A. J. Stace, H. W. Kroto, K. Hansen, and E. E. B. Campbell, Int. J. Mass Spectrom. Ion Processes **167/168**, 127 (1997).
[21] B. Concina, S. Tomita, J. U. Andersen, and P. Hvelplund, Eur. Phys. J. D **34**, 191 (2005).
[22] K. Głuch, S. Matt-Leubner, O. Echt, B. Concina, P. Scheier, and T. D. Märk, J. Chem. Phys. **121**, 2137 (2004).
[23] B. Concina, K. Głuch, S. Matt-Leubner, O. Echt, P. Scheier, and T. D. Märk, Chem. Phys. Lett. **407**, 464 (2005).
[24] J. U. Andersen, E. Bonderup, and K. Hansen, J. Phys. B **35**, R1 (2002); http://fy.chalmers.se/~klavs/statfys.pdf.
[25] K. Hansen, *Statistical Physics of Nanoparticles* (Göteborg, 2003).
[26] K. Hansen and E. E. B. Campbell, Phys. Rev. E **58**, 5477 (1998).
[27] K. Hansen and L. Schweikhard, *Encyclopedia of Mass Spectrometry* (Elsevier, Amsterdam, 2003), Chap. Metal Clusters.
[28] W. A. de Heer, Rev. Mod. Phys. **65**, 611 (1993).
[29] I. V. Hertel, H. Steger, J. de Vries, B. Weissner, C. Menzel, B. Kamke, and W. Kamke, Phys. Rev. Lett. **68**, 784 (1992).
[30] J. Borggreen, P. Chowdhury, N. Kebaïli, L. Lundsberg-Nielsen, K. Lützenkirchen, M. B. Nielsen, J. Pedersen, and H. D. Rasmussen, Phys. Rev. B **48**, 17507 (1993).